

Insight into the impacts of acid and base pre-treatment on activated carbon and biochar electrodes in flow-electrode capacitive deionization

Hanna Jaroszek^a, Anna Siekierka^b, Paulina Copik^a, Agnieszka Korus^{a,*}

^aDepartment of Thermal Technology, Silesian University of Technology, Konarskiego 22, 44-100 Gliwice, Poland;

emails: h.jaroszek@gmail.com (H. Jaroszek), paulina.wienchol@polsl.pl (P. Copik), agnieszka.korus@polsl.pl (A. Korus)

^bDepartment of Process Engineering and Technology of Polymer and Carbon Materials, Wrocław University of Science and Technology, Wyb. St. Wyspiańskiego 27, 50-370 Wrocław, Poland, email: anna.siekierka@pwr.edu.pl (A. Siekierka)

Received 27 June 2023; Accepted 15 October 2023

ABSTRACT

Biochar is an abundant, yet highly heterogeneous, green alternative to the commercial activated carbons. As received, biochar possesses labile, soluble compounds that might obscure its utilisation in aqueous environments, for example, as porous electrodes for capacitive deionization. We investigated the effect of acid–base leaching on the physicochemical and electrochemical properties of straw biochar and commercial activated carbon. The findings suggested that the most commonly evaluated properties of the electrode materials (i.e., capacitance, resistance, functional groups, and porosity) do not unequivocally determine the electrode performance. The results point towards the importance of the more indefinite carbon properties, which differ between the pristine materials, arising from their inherent structural features, and could be related to their proton donating/accepting ability.

Keywords: Biochar; Activated carbon; Flow-electrode capacitive deionization; Acid/base pre-treatment; Flow carbon electrode

1. Introduction

In the face of the energy transition and increasing relevance of the renewable fuel synthesis, biochar, as an inextricable side product of bio-oil and syngas production, has been gaining much scientific interest [1–5]. In particular, biochar might become a green alternative to the conventionally produced carbons in modern materials [3,6,7], that is, in energy storage applications [8] or as porous electrodes [7,9]. Solid residues from biomass gasification are often highly porous and conductive [3,10,11], which advocates their suitability for ion electrosorption, for example, in capacitive water deionization.

Flow-electrode capacitive deionization (FCDI), an electrochemically driven process utilizing flowing carbon electrode, is gaining interest as a possible alternative to the traditional desalination processes, such as electrodialysis and

reverse osmosis [12–14]. In the most typical variant, FCDI is conducted in a three-chamber module. Each chamber is separated by ion-exchange membrane (IEM), which role is both to separate the process streams and to allow selective transport of ions from the diluate to the adjacent electrode chambers. As a result, the diluate stream gets deionised. The flow-electrodes – the suspension of carbon particles in an electrolyte – are charged by external electrical potential applied. According to the polarization, the carbon electrode became negatively (cathode) or positively (anode) charged and ready to sorb cations and anions, respectively, in the electric double layer (EDL). Besides process parameters, such as operational mode, applied voltage, salt concentration, the efficiency of the FCDI process depends largely upon the properties of the flow-electrode [13–18]. Desired characteristics of the active material for flow-electrode are: large specific surface area, high capacitance, good conductivity,

* Corresponding author.

low cost, good wettability, high ion selectivity, good suspension flowability and stability [13,19,20].

Biochars properties makes them promising materials for flow-electrodes in FCDI [9]. For example, biochar obtained from the two-stage gasification of spruce not only possessed high surface area exceeding 1,200 cm²/g, it also has almost 50/50 split between micro and mesopores, making it good catalytic material that was resistant to deactivation [21]. However, the heterogeneity of the gasification biochar, including inherent inorganic compounds, might become an obstacle in its direct use as the electrode material. Biochar has an abundance of the labile species that are not part of the carbon framework, and might dissolve in the electrolyte solution, interfering with the deionisation process.

Numerous pre-treatment procedures aimed at increasing electrode capacitance (by surface functionalisation and porosity development) [22–24] and at improving the conductivity of the electrode material [25] have been used on the commercial carbons. Thus far, a limited number of studies on the biochar flow-electrodes has been performed [9], and these did not include any modifications or pre-treatments. Meanwhile, biochars are particularly heterogeneous materials with high inorganic content, and a variety of surface functionalities and lighter aromatics remaining after the feedstock devolatilization [11,26]. Thus, biochar-based electrodes might particularly benefit from the leaching pre-treatment that would remove the labile compounds. Typically, the acid wash is used for inorganic removal, while organic acids, phenols, and humic-like substances can be dissolved in basic solutions [27–29].

Examining the effect of the labile species on the biochar electrochemical performance will contribute new insight into the potential of using these types of carbon as the electrode material. In this paper, we examined the properties and the FCDI performance of the commercial carbon and gasification biochar electrodes after the pre-treatment aimed at labile compounds and acid-soluble inorganics removal, and the saturation of the carbon surface charge. The procedure involved consecutive acid and base leaching, followed by the protonation with diluted acid, and the water rinsing.

2. Experimental

2.1. Materials and pre-treatment

All chemical reagents, with ACS reagent grade or higher, used for carbon pre-treatment and analyses, and the desalination tests (HCl, NaOH, NaCl, etc.) were purchased from Merck KGaA, Darmstadt, Germany. High purity gases (99.9999%) for the gas adsorption tests were delivered by Air Liquide Polska, Kraków, Poland.

Two types of carbon were examined as the electrode material. For the reference, the wood-derived commercial activated carbon, type CWZ-22 was used (denoted as AC). The biochar (denoted as BC) was prepared from the straw pellet in the two-stage gasifier operating at the Technical University of Denmark (DTU) Risø, in Roskilde, Denmark [30].

Both carbons were air-dried at 40°C. Each material was used directly (BC and AC) or after the leaching pre-treatment

(denoted as BC-L and AC-L) proposed by Tsechansky and Graber [27]. The procedure involved consecutive leaching with the acidic and alkaline aqueous solution (at room temperature) to remove any soluble constituents and compounds that are not bound to the carbon matrix. The raw material was shaken for 24 h in the 0.05 M HCl solution, rinsed with distilled water, shaken for another 24 h in 0.05 NaOH, and rinsed again. Finally, the sample was protonated by the 24 h wash in 0.025 M HCl, rinsed with deionised water and air-dried at 40°C.

2.2. Analyses of carbon properties

Sorption and desorption tests were conducted to estimate the effect of electrode solution on carbon materials: 50 ml of 5% carbon material slurry in either: 3%wt. NaCl or deionised water was shaken for 12 h. pH and concentrations of Na, K, and Cl ions were measured in solutions in equilibrium with carbon material sample.

Particle size analysis was done by laser diffraction method on Shimadzu SALD-7500, measuring particles in the range from 7 nm to 800 μm.

The porosity of the carbons was evaluated with the gas adsorption method. Isotherms of N₂ adsorption at 77 K and CO₂ at 273 K were measured with Micromeritics TriStar II 3020 analyser after degassing the samples in N₂ flow at 200°C for 24 h. Two theoretical NLDFT models were simultaneously fitted to the corresponding experimental isotherms to calculate the pore size distribution (PSD) in each carbon, using the numerical algorithm SAIEUS [31]. The dedicated models for the carbon slit-shaped pores with surface energetical heterogeneity, developed by Jagiello and Olivier [32], were used to avoid artifacts that are often present in PSDs of turbostratic carbons when standard models are used. The carbon samples' total pore volume and total surface area were calculated as integrals of the dual 2D-NLDFT surface and volume distributions in the 3.6–500 Å pore size range.

The surface functional groups on the carbons were investigated with FTIR spectroscopy using Perkin Elmer Spectrum 100 with an ATR module. In addition, surface elemental composition was also assessed with SEM-EDS, using FEI Quanta 250 FEG microscope with Octane SDD detector.

Electrochemical impedance spectroscopy (EIS) was applied for resistance determination. The PTC1TM Paint Test Cell was used for testing. The sample was placed in the titanium flat sample and covered by PortHoles™ to expose 0.785 cm² of the active surface. The platinum wire was used as a counter electrode, and the 3 M Ag/AgCl system as a reference electrode. The testing solution was used individually for 3 wt.% NaCl in DI water (20 mL). The EIS was performed using potentiostat/galvanostat/ZRA Interface 1010T from Gamry Instruments. Oscillation frequencies were swept from 0.01 × 10¹ Hz to 2 × 10⁴ Hz. The EIS spectra were analysed using Gamry Echem Analyst software. The cyclic voltammetry was performed using the same setup as EIS measurements. The potential range was about –0.2 to 0.2 V with a scan rate of 40, 20 and 10 mV/s.

The specific capacitance was calculated according to Eq. (1):

$$C_{sp} = \frac{\int IdV}{vm\Delta V} \quad (1)$$

where C_{sp} is the specific capacitance of the capacitor (F/g), I is the instantaneous current (A), ΔV is a potential window width (V), m is the mass of active material (g), v is the potential scan rate (V/s), and $\int IdV$ is the total volumetric charge obtained by integration of positive and negative sweep in cyclic voltammetry.

Zeta potential analyses were realized using a Zetasizer Nano ZS analyser. All measurements were performed at room temperature. The samples were dispersed in 3 wt.% NaCl at the concentration of 1 mg/mL and sonicated for 3 min using an ultrasonic bath. The pH titration sequence started from decrease of pH to 2.0 by HCl, and subsequently, pH increase by KOH in steps by pH 0.5, up to pH 11.0. For each pH point, three zeta potential measurements were done. Because of high medium conductivity, all zeta measurements were done using the monomodal mode of analysis, which allowed to obtain average zeta potential value without its full distribution.

2.3. FCDI experiments

3-chamber FCDI cell was used in this study. Neosepta AMX and CMX ion-exchange membranes (ion transport number > 0.98) separated electrode chambers and a desalination chamber. Graphite current collectors with serpentine channels as described by Tang et al. [19], of 84.5 cm² of cross-section area and 43.2 cm² of active area, were used, with the diluate compartment of 0.5 mm thick, equipped with PP spacer.

Isolated current cycle (ICC) operation mode was used: 10 ml of diluate solution (model brackish water: 30 g NaCl/L) and 50 ml of each (separated) electrode solution were recirculated via a supply tank through an FCDI module with flow rate of 6.5 and 2.4 mL/min, respectively. Electrode solutions were stirred to prevent settling of carbon particles. An electrical potential was provided to the FCDI system by a DC power supply (GPP-2323, Gwinstek), and the current response of the FCDI device was continuously monitored with 1 s intervals. Each experiment duration was 2 h. Conductivity of diluate solution was monitored every 10 s with conductometer (CC-401, Hydromet) equipped with flow-chamber electrode (CFT-21, Hydromet).

In this work we compared biochar and active carbon performance in FCDI process operated either in constant voltage or constant current mode. Moreover, electro dialysis tests were conducted under the same conditions to compare its desalination properties with FCDI process. In ED experiments electrode solution was 3%wt. NaCl. In FCDI experiments electrode was composed of 5%wt. of carbon material in 3%wt. NaCl. In constant voltage experiments, 1.2 V was used and in constant current experiments, 65 mA (corresponding to current density of 15 A/m²), instead of constant voltage, was provided.

Current/voltage and diluate conductivity were continuously measured during each test run. However, due to the considerable changes in pH (SI), the final NaCl concentration in diluate was measured post-run with ion chromatography,

and this value was used to determine desalination efficiency parameters in Eqs. (2)–(4).

After each experiment spent carbon materials were filtered from electrode solutions through 0.45 μm filter and air-dried at 40°C for at least 48 h.

pH values of FCDI solutions were measured with Mettler Toledo SevenCompact Duo equipped with InLab ExpertPro-ISM electrode. Concentrations of ions (Na, Cl, K) were determined by ion-chromatography system ICS-5000 (Thermo Dionex, USA) equipped with AS-19 anion-exchange and CS-16 cation-exchange columns operated in a suppressed conductivity mode.

The performance an of the FCDI processes was assessed using the following parameters:

Effective current efficiency, calculated as:

$$CE_{eff} = 100 \frac{Fz(C_0V_0 - C_tV_t)}{\int_0^t I(t)dt} \quad (2)$$

Average salt removal rate, calculated as:

$$ASRR = \frac{C_0V_0 - C_tV_t}{At} \quad (3)$$

Energy consumption, calculated as:

$$EC = \frac{\int_0^t UI dt}{(C_0V_0 - C_tV_t)} \quad (4)$$

where I – electrical current (A), t – operation time (s), A – effective contact area (cm²), F – Faraday constant, (C/mol), C_0 and C_t – the initial NaCl concentration and final NaCl concentration in the diluate stream (mol/L), V – volume of the salt solution (L), U – voltage (V).

3. Results and discussion

3.1. Physicochemical properties of the carbons

The leaching procedure applied herein consist of three steps: acid treatment – to solubilize and remove basic minerals and species, base treatment – to solubilize and remove organic and inorganic acids, and again with acid – to protonate acidic carbon sites [27]. Pre-treatment should remove the interfering species but not oxidise carbon surface.

Median particle diameter (Table 1) was in the range typically used for flow-electrode suspensions, and it was similar for both carbon materials. The pre-treatment had no significant effect on particle diameter.

Surface area calculated with the BET model based on the N₂ adsorption isotherm is presented in Table 1 to enable literature comparison. However, the discussion on pore development was based on the pore size distribution (PSD) obtained with dual 2D-NLDFT models as it enables more thorough investigation of ultramicropores using CO₂ as the probe molecule.

Detailed PSDs are presented in Fig. 1, model based cumulative (total) pore volume and surface area are provided in Table 1. Compared with biochar, AC had significantly more

Table 1
Physicochemical characteristics of carbon materials in study

Material	Median particle size, μm	BET surface area, m^2/g	Dual 2D-NLDFT cumulative surface area, m^2/g	Dual 2D-NLDFT cumulative pore volume, cm^3/g
BC	18	570	700	0.28
BC-L	18	692	859	0.36
AC	16	945	1068	0.47
AC-L	15	960	1088	0.48

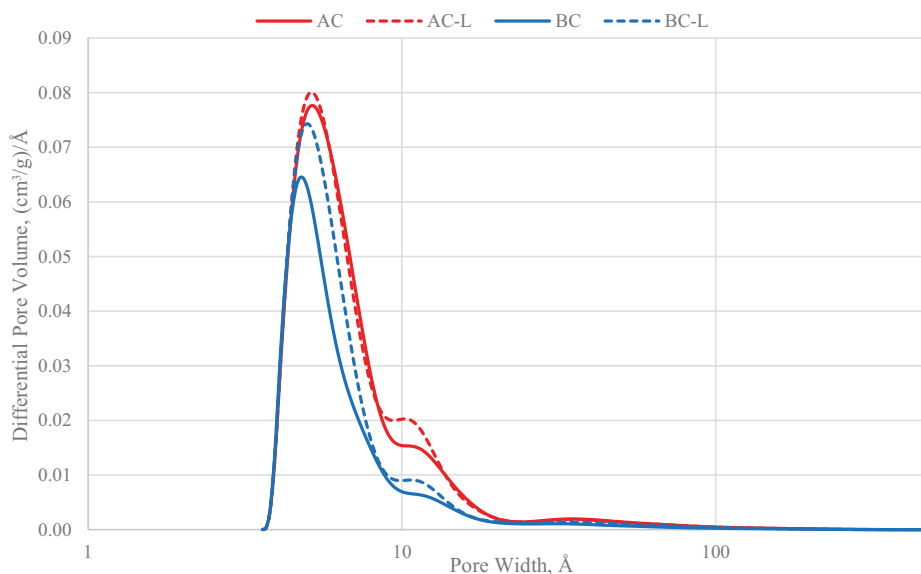


Fig. 1. Pore size distribution in raw and leached carbons calculated with dual 2D-NLDFT models.

developed porosity in all pore size ranges, though the structure of both samples was highly microporous, with dominating ultramicropores ($< 7 \text{ \AA}$), and some supermicropores ($7\text{--}20 \text{ \AA}$). The leaching pre-treatment was likely to remove part of the inorganic and labile organic compounds, increasing pores accessibility and widening them. Biochar treatment enhanced its surface area and generally increased the porosity, without favouring any particular pore type. Contrarily, the leaching of AC increased mainly supermicropores, which have relatively small contribution to the overall surface area, yet much better accessibility, compared with ultramicropores that are often too narrow to facilitate the hydrated ion with diameter of approx. 7 \AA , such as Na^+ [7]. Thus, as the general trend of applied pre-treatment was carbon porosity development, the subtle differences in how the leaching affected different pore types in each sample might change the significance of leaching to the sorption enhancement.

The ATR-FTIR analysis revealed that leaching also affected the surface chemistry of the studied carbons (Fig. 2). Each raw sample had a distinct spectrum suggesting specific functional groups, which were altered during the treatment. AC, beside the skeletal carbon, had some O-containing functional groups, such as single bonded O, for example, in ethers, giving rise to the broad band around $1,000 \text{ cm}^{-1}$. The increased absorption in the region between $1,600$ and

$1,350 \text{ cm}^{-1}$ could be attributed to aromatic structures as well as C–O bonds in the resonance-stabilised structures, for example, semiquinones [33]. The BC spectrum was characterised by the more intense absorption at similar wavelengths. Here, the band at fingerprint region could also be indicative of the C–O and skeletal C–C bonds. However, Si–O bonds most likely have a significant contribution to the absorption around $1,000 \text{ cm}^{-1}$ [34], as the SEM-EDS analysis confirmed biochar surface was abundant in silica. For AC, the leaching resulted in the decreased absorption around $1,400 \text{ cm}^{-1}$, suggesting that the acid/base treatment might have saturate some aromatic and resonance-stabilised structures. On the other hand, an increase in number of –OH groups was observed in the BC-L spectrum ($3,600\text{--}3,000 \text{ cm}^{-1}$) [35], which, along with the enhanced absorption in the fingerprint region, suggested that the protonation of some oxygen functional groups, resulting in alcohols and/or phenols formation, occurred during the treatment.

Surface chemistry of the samples was further investigated with the SEM-EDS analysis (Fig. 3). The micrographs for all carbons are provided in the Supplementary Information (SI). The surface of the AC was typical for wood-derived chars, with the remnants of the original wood tissue structures, such as open pores and groves from wood cells and channels decomposition [36]. No visible effects of leaching and no change in surface chemical

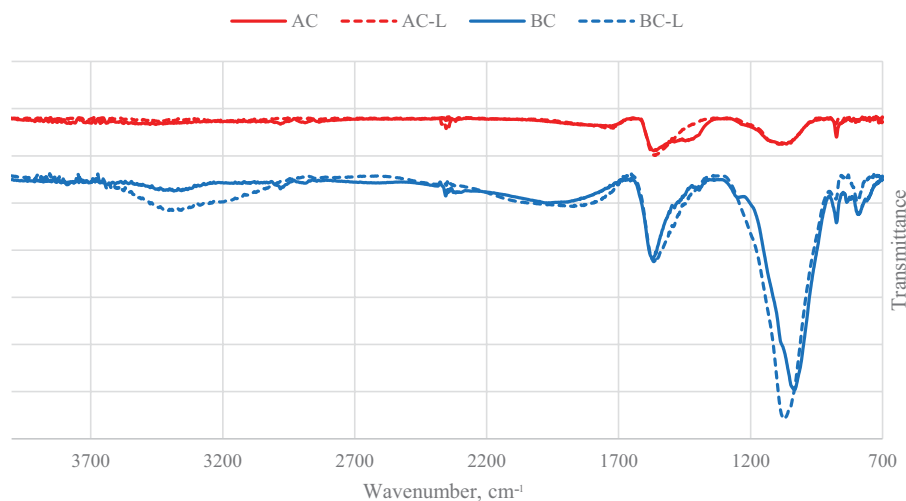


Fig. 2. ATR-FTIR spectra of the raw and leached carbons.

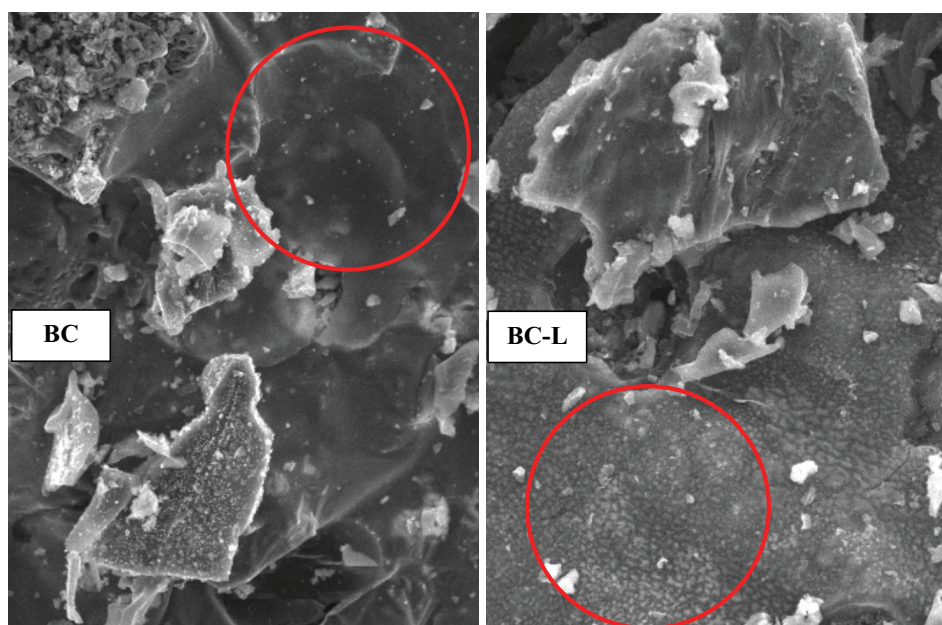


Fig. 3. SEM micrographs of the raw (BC) and leached (BC-L) biochar with the indicated changes in the roughness of the surface (red circles).

composition were observed in micrographs and EDS mapping (Fig. 4) of this material. On the other hand, the surface of the straw biochar became much rougher after the leaching, as indicated by the red circles in Fig. 3.

The composition of the carbon surface was also investigated. The mapping of the carbons is presented in Fig. 4 and the detailed composition is provided in the SI. Biochar (BC), as received from the gasifier, was abundant in inorganic compounds, particularly Si and Fe, which were largely removed during the pre-treatment step. As the commercial production of activated carbons involves chemical treatment, the raw AC sample already had a limited diversity of the inorganics, thus the leaching did not affect its composition.

3.2. Electrochemical properties of the carbons

The EIS and CV measurements were aimed at determination of the electrochemical properties of the carbons, such as capacitance and resistance. The CV profiles of all samples (Fig. 5) differed from the rectangular shape characteristic an ideal supercapacitor. All CV profiles had blunted edges and were slanting, particularly the raw carbons. Using the equivalent circuit analysis, Boonpakdee et al. [37] described these deviations using the equivalent serial and parallel resistances. For both investigated materials, the leaching resulted in more rectangular CV profiles, suggesting lower equivalent resistance and thus more capacitive-like behaviour.

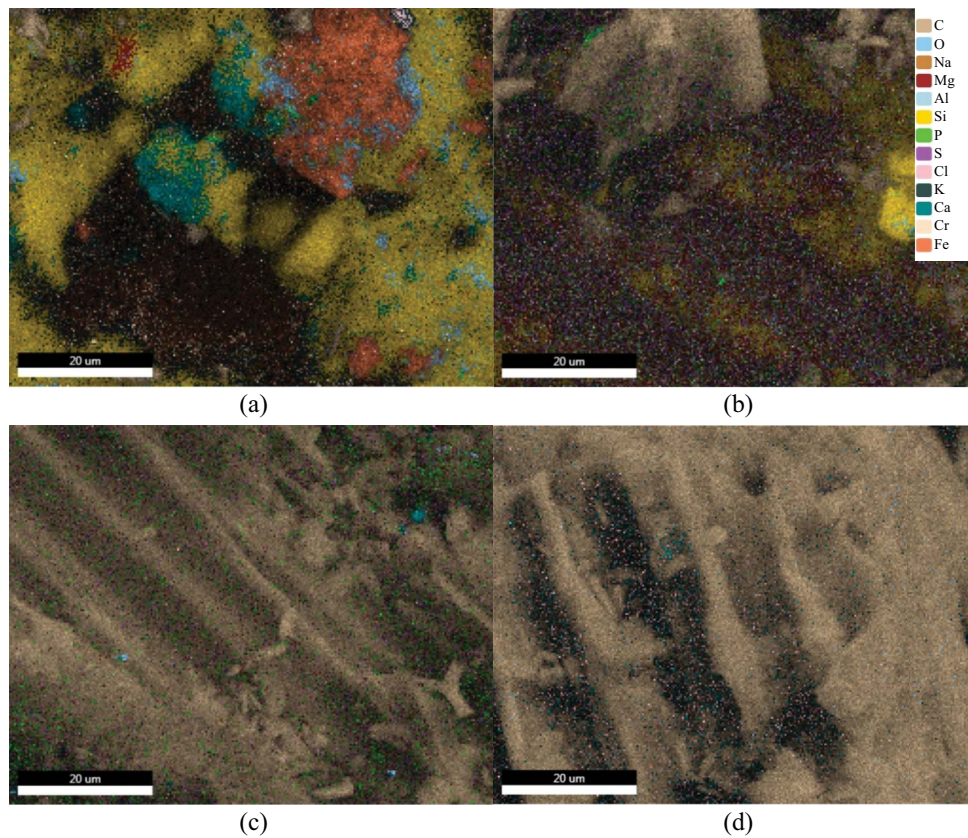


Fig. 4. SEM-EDS mapping of the carbon surface of the (a) BC, (b) BC-L, (c) AC, and (d) AC-L carbon surface.

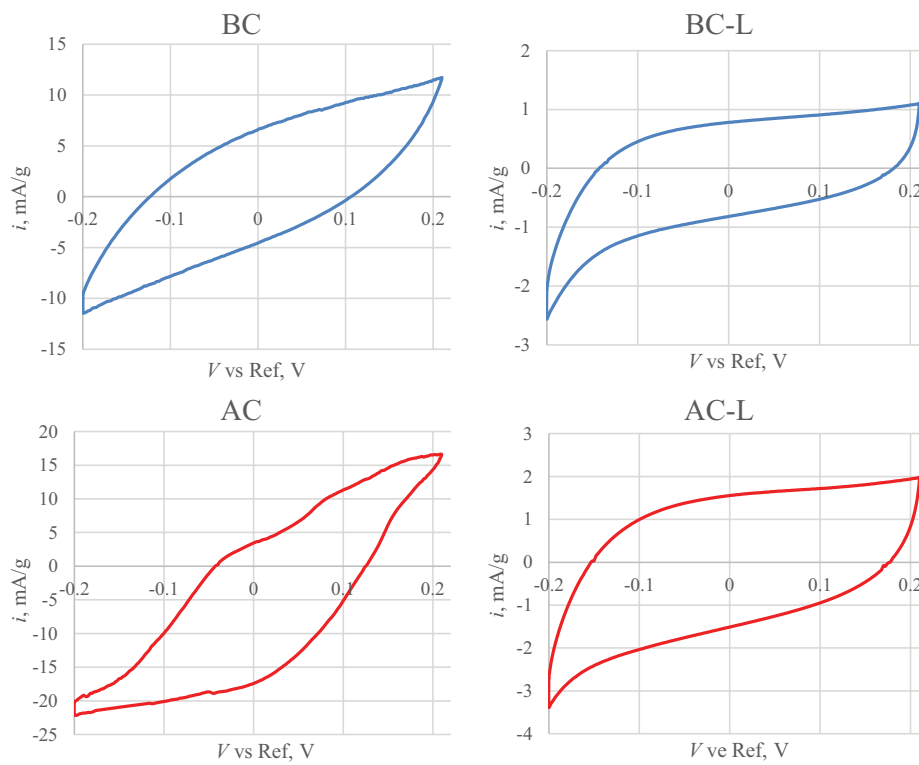


Fig. 5. CV profiles for 10 mV/s scan rate.

The capacitance calculated for the 10 mV/s scan rate is provided in Table 2 along with the carbon resistance modelled with the equivalent circuit. The leaching resulted in a significant drop in the specific capacitances of both carbons, despite the more rectangular shape of their CV plots. The non-ideal capacitive properties of the carbons were further investigated by the calculation of the contribution of electrical double layer and diffusion-limited processes in the charge storage mechanism (Fig. 6). To this end, the relationship between voltametric current and sweep rate was investigated at the current peak of the CV plots, according to the method described by Forghani et. al. [38]. The analysis of the current response to the change in the sweep rate aligned with the characteristics of the CV profiles. For the raw carbons, especially BC, the kinetics were almost entirely governed by diffusion processes, while in the BC-L and AC-L materials the electrical double-layer significantly contributed to the charging mechanism. All capacitances were also rapidly decreasing with the scan rate (SI), supporting the notion of the diffusion-governed kinetics of the charging process. These results suggest that in both carbons the pseudocapacitive processes dominated the ion capturing. The leaching pre-treatment is expected to decrease the number of reactive sites on the carbon surface, thus inhibiting the pseudocapacitive mechanism, resulting in the lower specific capacitance but increasing the role of the EDL in the BC-L and AC-L carbons.

The leaching had also a visible effect on the electrical resistance of the biochar. The resistance calculated for the BC-L electrode was almost two times smaller than of the BC. The most plausible explanation is the high content of inorganics present in the raw biochar and their significant removal during the pre-treatment, as observed from SEM-EDS analysis.

Zeta potential of the carbon surface was measured in the 3 wt.% solution of NaCl at different pH values (Fig. 7). Interestingly, all the samples were characterised by the positive zeta potential in the pH range of 3–9 and negative potential otherwise. Unfortunately, the nature of the surface charge cannot be unequivocally determined based on the zeta potential [39]. One of the plausible causes for the zeta potential reversal is the overcharging that can occur at high ionic strength conditions, when the counterion local density is so high it compensates the particle charge [40]. At high electrolyte concentration zeta potential values are rather low, as was also observed in this case. Low absolute values of the potential (< 30 mV and > -30 mV) indicate that the particles have a tendency to agglomerate [41]. With this in mind, generally lower BC zeta potential, compared with AC, indicates that the later formed more stable colloid suspension.

Table 2
Resistance and specific capacitance of raw and leached carbons

	Resistance, Ω	Specific capacitance, F/g
BC	50.09	90.06
BC-L	25.56	14.33
AC	16.54	123.88
AC-L	15.45	27.75

The leaching slightly affected the behaviour of the samples at alkaline environment. Zeta potential of BC-L was more positive at $\text{pH} < 9$ and less negative at $\text{pH} > 9$, compared with the untreated sample (BC). Contrarily, activated carbon leaching resulted in the decrease of its zeta potential, that is, the less positive values below $\text{pH} 9$ and more negative at $\text{pH} > 9$. Nevertheless, the changes were relatively small and the results do not indicate any relevant differences in the electrophoretic mobility of the four examined carbon suspensions.

3.3. FCDI experiments

Desalination tests were performed using raw (BC, AC) or pre-treated (BC-L, AC-L) carbons as flow electrodes. Salt removal was investigated in the constant voltage (C.V.) and constant current (C.C.) modes, as detailed in section 2.3. Test runs without carbon suspension, that is, electro dialysis (ED), for each mode were considered as the reference for carbon electrodes performance.

In the C.V. mode the current is resulting from the total resistances of system components. The changes of current during the C.V. operational mode of FCDI (Fig. 8a) were typical for the FCDI isolated closed-cycle (ICC) process. The initially decreasing current reflects the charging of the porous electrode. Then, current stabilizes and reaches quasi-steady state, in which process become similar to electro dialysis, where ions are transported through IEMs to the electrode compartments and retained there [42]. The final current value varied for different electrode materials due to the total resistance of the system (mostly differing in carbon and diluate ohmic resistances), resulting in different desalination efficiency [43] – in both examined cases leached carbons performed better when used as electrode material.

In the C.C. operational mode, constant current is maintained throughout the process, providing constant desalination rate, and the cell voltage is the resultant. Observed voltage increase (Fig. 8b) was typical for the ICC setup of FCDI – the steep initial increase leading to a quasi-steady value (the final slight increase is resulting from increasing resistance of the diluate as it desalinates). The smooth increase in voltage was observed in the cases where leached materials were used. The step-like change in voltage during the FCDI with raw carbons suggests the occurrence of few

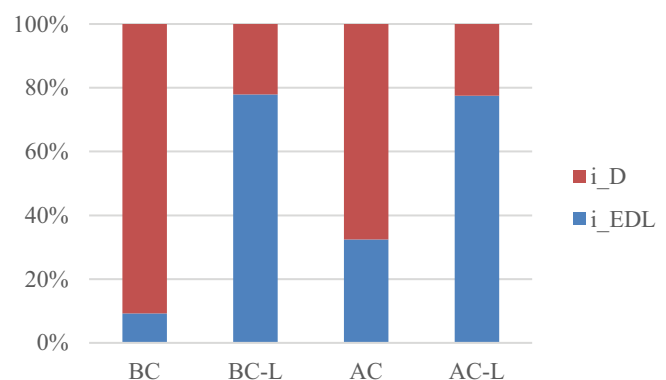


Fig. 6. Contribution of the electrical double layer (i_{EDL}) and diffusion-limited (i_D) current at the current peak at maximum potential for the 10 mV/s sweep rate CV profile.

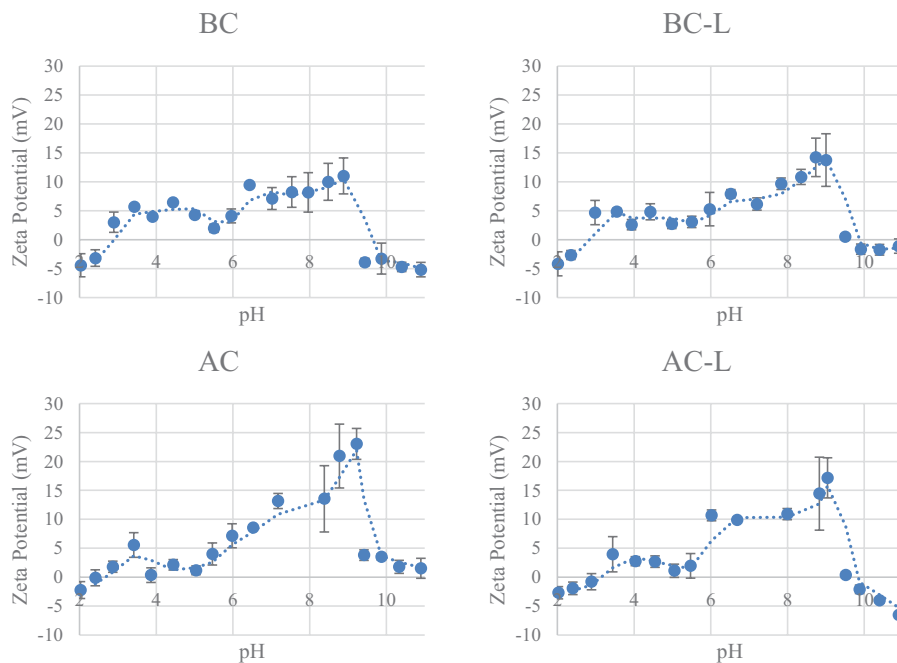


Fig. 7. Zeta potential of the carbons as a function of pH.

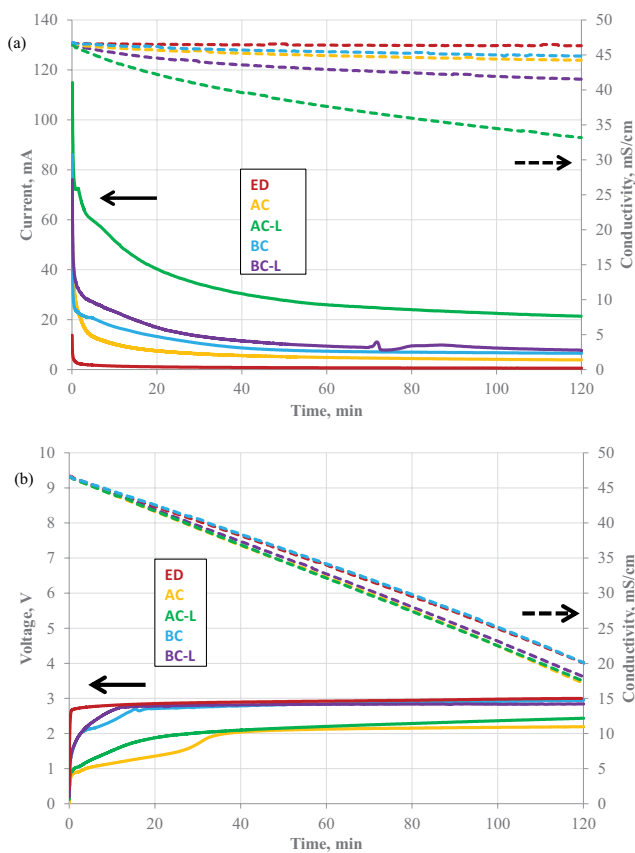


Fig. 8. Changes of voltage (solid line) and conductivity of diluate (dashed line) during FCDI process in (a) C.V. mode ($U = \text{const. } 1.2 \text{ V}$) and (b) C.C. mode ($I = \text{const. } 65 \text{ mA}$); $c_{0, \text{NaCl}} = \text{wt.3\%}$ (diluate and electrolytes).

consecutive processes, taking place at different voltages. These may be related to the different EDL storage channels [37] and/or the faradaic redox reactions. The occurrence of Faradaic reactions in all C.C. tests was expected because the process voltage exceeded water's decomposition voltage. It was also confirmed by the changes in the FTIR spectra of the electrode material used in this operational mode (SI).

In both operational modes the reference ED tests had significantly lower process efficiency—compared to the runs with carbon suspension in the electrodes, which confirms the important role of carbon in facilitating charge transfer in the FCDI system. It is generally believed that electrons – the charge carriers – are transported by the direct contact between the current collector and carbon particles, or through the network of contacting carbon particles; the latter depends largely on the carbon load in the electrode [14].

Electrical charge transferred through the FCDI module corresponds with the desalination rate, observed as the decrease in diluate conductivity. However, the effective current efficiency (CE), that is, how much of the charge transferred through the system was used for the transport of ions from the diluate compartment into the electrode, was in the range of 60%–80%. Typically, $CE > 80\%$ is desired in electrochemical processes, to minimize energy consumption, and thus, operating cost. The loss of current can be result of shunt currents between the electrodes in stack or back-diffusion of species, declining the effective flux of ions. However, in FCDI the loss of current is usually attributed to the presence of parasitic faradaic reactions. One of the most plausible to occur is carbon oxidation [14] due to a relatively low potential required (Table 3). Both raw carbon materials performed similarly in terms of current utilization, and leaching in both cases improved CE in the C.V. mode and showed little effect the C.C. mode.

Average salt removal rate (ASRR), a measure of kinetic desalination efficiency by FCDI module, is defined as the amount of salt removed by a unit of membrane area in a unit of time. In all cases (Fig. 9), ASRR was the lowest in the reference ED process, and lower in C.V. than in the C.C. mode where, due to the constant current density applied to electrodes, the ion transport rate does not decrease with time. BC-based electrodes performed better than AC-based, and for both materials leaching increased ASRR; this effect was the largest in case of AC-L, which provided the best kinetic desalination efficiency in the study.

Faradaic reactions are often overlooked in FCDI studies. Maintaining constant voltage below water’s decomposition voltage (1.23 V) is considered an effective way to avoid Faradaic reactions, however, many studies report Faradaic reactions occurrence nonetheless [44,45]. Faradaic half-reactions that are plausible for the system in study (comprising water NaCl solution and carbon electrodes) are shown in Table 3. Most of them will lead to the generation of charged species (H⁺, OH⁻) that affect pH and can explain observed changes in pH of the electrode solutions. Redox reactions can also alter the surface chemistry of the carbon

electrode particles. Mass loss and pore structure deterioration of carbon electrodes due to carbon oxidation at anode were reported earlier in CDI [46,47] and this reaction is likely to occur preferentially at anode due to its relatively low standard redox potential.

All carbons, and raw ones in particular, strongly alkalinised the electrolyte solution (SI). Therefore, the pH changes occurring during the FCDI tests should be considered in respect to the initial pH values of electrolytes and diluate (Fig. 10). In all variants of the FCDI process in study, pH of anode decreased – became more acidic, and of cathode increased – became more basic. This observation aligns with the notion of Faradaic reactions occurring on both electrodes, even under potential below 1.2 V. However, the pH changes were much higher in case of the C.C. mode, where, due to process voltage, Faradaic reactions were inevitable.

As the electrolyte solution with carbon suspension at equilibrium was strongly basic, any H⁺ ions that might be generated during the cathodic water oxidation would become neutralized. Nevertheless, generation of H⁺ ions in anode compartment is apparent from the observed pH decrease and, as expected, it was more intense in C.C. mode due to the generally larger charge generated during process. Final anode pH in C.C. mode were all slightly above 12, which is apparently a limiting value for anion membrane in study and all excess OH⁻ ions are transported back to diluate (as limiting value is linked with concentration, the mechanism is probably NaOH back diffusion).

Since redox reactions occur only in the electrode compartments, either on carbon electrodes or at the current collector interface, the pH changes measured in the diluate are the result of the back-migration of H⁺ and/or OH⁻ ions [42,45]. In all FCDI processes in study the diluate became

Table 3
Most common redox reactions to occur on carbon electrodes in FCDI and their standard electrode potentials

Cathode (reduction):	$2H_2O + 2e^- \rightarrow H_2 + 2OH^-$	$E^\circ = -0.83\text{ V}$
	$C + 2H_2O \rightarrow CO_2 + 4H^+ + 4e^-$	$E^\circ = +0.21\text{ V}$
Anode (oxidation)	$2H_2O \rightarrow O_2 + 4H^+ + 4e^-$	$E^\circ = +1.23\text{ V}$
	$2Cl^- \rightarrow Cl_2 + 2e^-$	$E^\circ = +1.36\text{ V}$

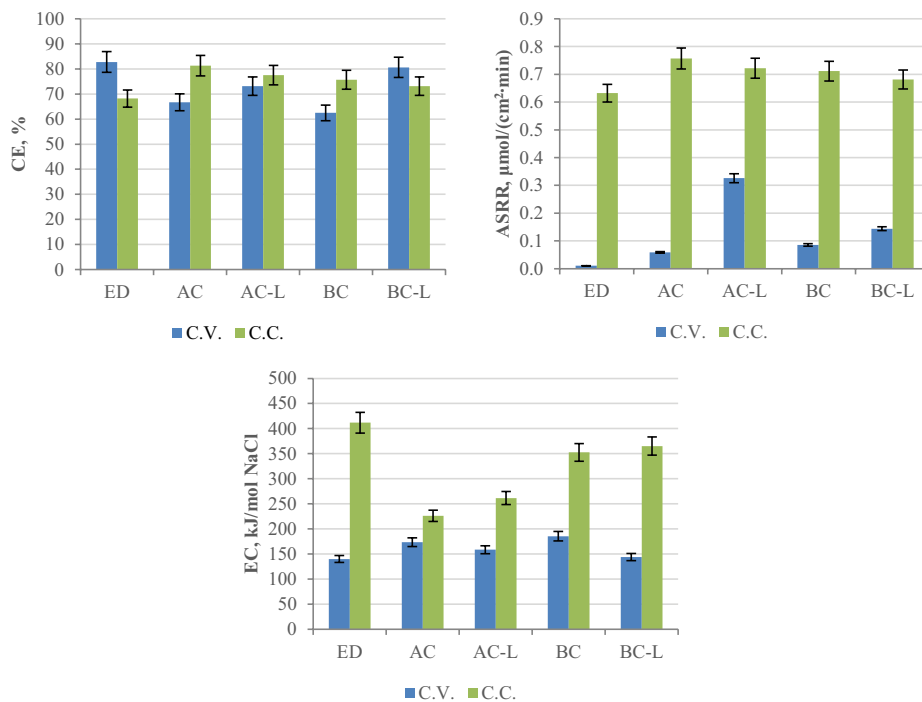


Fig. 9. Performance indicators of FCDI processes: current efficiency (CE), average salt removal rate (ASRR) and energy consumption (EC).

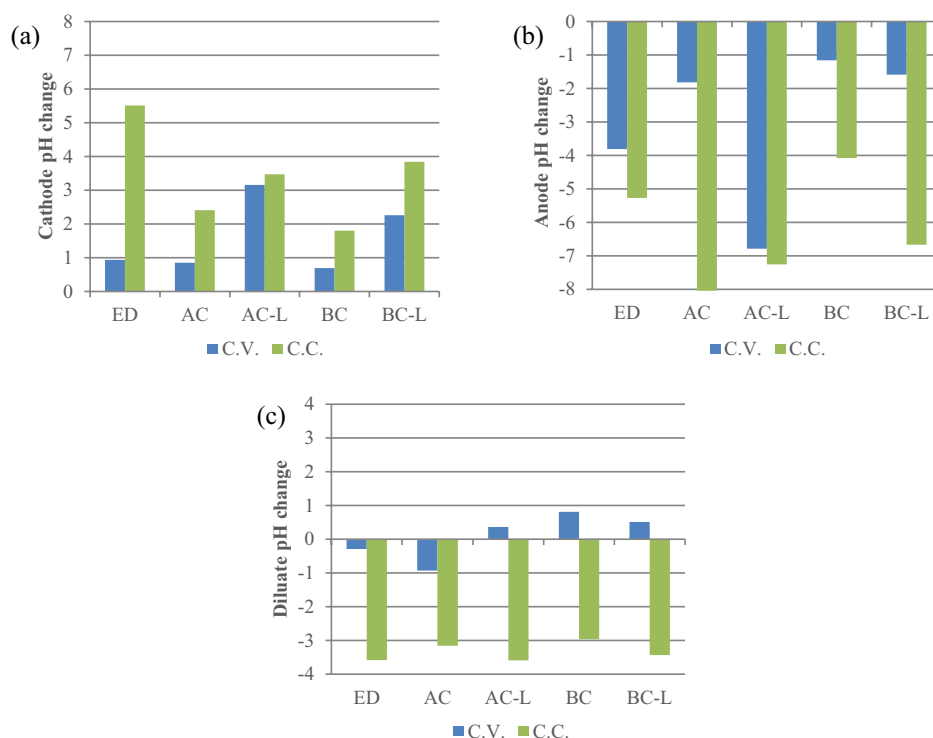


Fig. 10. Changes of pH of process solutions during FCDI (relative to an electrolyte solution in equilibrium).

acidic, due to the back-migration of mobile hydrogen ion generated on the anode. The mobility of H^+ ion is nearly twice that of the OH^- ion [48].

Based on the measured zeta potentials (Fig. 7), investigated carbons had positive potential in the pH range of 3–9. Considering measured pH values, for BC the pH changes during process were favourable for electrode potentials. However, AC seems to be more suitable for anode than cathode (having better affinity to anions), while the opposite can be expected of AC-L. This can potentially lead to differences in capacity for ions between cathodes and anodes, as observed by Ma et al. [42].

3.4. Role of leaching

The presence of carbon in flow-electrodes generally enhanced the efficiency of the desalination process under the constant current (C.C.) mode, compared to ED. However, no significant differences in the performance between the raw and pre-treated materials were observed. As this operational mode was governed by the Faradaic reactions, it was likely less sensitive to the properties of the carbons. The only apparent differentiation between the samples was in the energy consumption – C.C. tests with both activated carbons (AC and AC-L) had lower EC compared with biochar materials (BC and BC-L), in accordance with lower resistance of AC in study (Table 2), and thus, with the lower voltage at which the process stabilised (Fig. 9). Different conductivity of AC and BC likely results from differences in the core structure of these materials that was not altered by the leaching. The high resistance of BC can be attributed to its high inorganic content. Leaching partially removed the

non-conducting elements, such as silica [24], thus reducing the resistance of BC-L electrode.

As the resistance of flow electrodes, even for highly conductive saline set-up, stands a large share of the overall cell resistance (*c.a.*, 30% of potential drop [49]), it should be an important aspect of the desalination performance. Simultaneously, the capacitance of the porous electrode is considered to be determining the FCDI process efficiency. Although the lower resistance and higher capacitance of AC, compared with BC, could be responsible for its higher efficiency as the flow-electrode, another carbon properties must have a crucial impact on the desalination process. Almost twofold drop in the biochar resistance after the leaching pre-treatment aligns with the improved performance of BC-L in the C.V. modes, yet it does not alter the results of the C.C. tests. Moreover, even more pronounced improvement in the C.V. tests was observed for the activated carbon, despite a negligible reduce of the resistance of the leached material. Finally, most surprisingly, the specific capacitance of both carbons decreased dramatically after the leaching, yet the electrodes made of AC-L and BC-L performed much better than the raw carbon suspensions.

Some plausible explanations for the improved performance of the leached carbons lies in the changes in their surface chemistry and charging mechanisms. Pyrogenic carbons often have both electron donating and accepting active sites, such as quinones, semiquinones, and even environmentally persistent free radicals [6,50]. Moreover, the aromatic structures can facilitate further the electron transfer through the graphite-like sheets [6]. The presence of both donating and accepting sites on the investigated materials can be expected, based on the observed FTIR spectra and

the changes in zeta potential showing two isoelectric points. Thus, consecutively exposing the carbon surface to acidic and alkaline solutions might have saturated these active sites, on a one hand decreasing the pseudocapacitive abilities of the carbons, on the other enabling the diffusion into the porous structure of the chars. This is in accordance with the changes in the CV profiles and the increased share of the capacitive current during the leached carbons charging. Besides the observed changes in the surface chemistry that might be responsible for the increased accessibility of the carbon surface, the leaching also removed some labile compounds, emptying and widening carbon pores. Due to the fractal structure of the carbon pore network [51], it is plausible that even a small expansion in the larger pores might have greatly increase the accessibility of the smaller ones.

4. Conclusions

Physicochemical properties of the activated carbon and biochar before and after the pre-treatment involving leaching in acidic and alkaline solutions were investigated to assess the effect of this pre-treatment on the carbon performance as flow-electrode in capacitive deionisation. The tests were performed under two modes – constant voltage and constant current. The tests under low, constant voltage of 1.2 V revealed a strong influence of the pre-treatment on the electrode performance.

Both examined carbons had sufficient physicochemical properties to show electrocapacitive behaviour. Interestingly, despite better characteristic, raw activated carbon did not perform better than raw biochar during the desalination tests performed under the constant voltage.

Furthermore, the leaching resulted in the decrease in capacitance of both materials, yet their performance as flow-electrodes was significantly improved by this pre-treatment. The average salt removal rate of the biochar electrode increased 1.6 times, and for the leached activated carbon it was 5.5 times higher than for the raw material.

The CV and EIS analyses suggested that the leaching decreased the diffusion-limited mechanisms of carbon charging and their resistance. Simultaneously, increase in the porosity, removal of inorganics, and changes in the surface functional groups were observed in the leached carbons. Thus, it is plausible that the applied pre-treatment removed labile species from the carbon matrix and altered its surface chemistry, thus increasing pore accessibility and enhancing carbon's surface affinity towards ion adsorption.

The findings showed that despite well-developed porosity and high capacitance of the examined carbon materials, their performance during desalination tests was not governed by these properties alone. It is likely, that some more undetermined structural and chemical carbon features (e.g., unpaired electrons, resonance stabilised aromatic structures, graphitic-like sheets arrangement) might have an important effect on their performance as desalination electrodes. Thus, investigating carbon electrode structure on the molecular level might become an interesting pathway towards the further understanding of the processes such as FCDI.

Acknowledgements

The research leading to these results has received funding from the Norway Grants 2014–2021 through the National Centre for Research and Development. (Project no. NOR/SGS/FlowChar/0062/2020-01, “Flow electrodes from biomass-derived char”, acronym: FlowChar, Small Grant Scheme 2020 Call).

The authors would also like to express their gratitude to Claus Dalsgaard Jensen from Technical University of Denmark for providing the biochar material, as well as Łukasz Majchrzycki and Marek Nowicki from the Centre of Advanced Technologies UAM for zeta potential and SEM-EDS analyses.

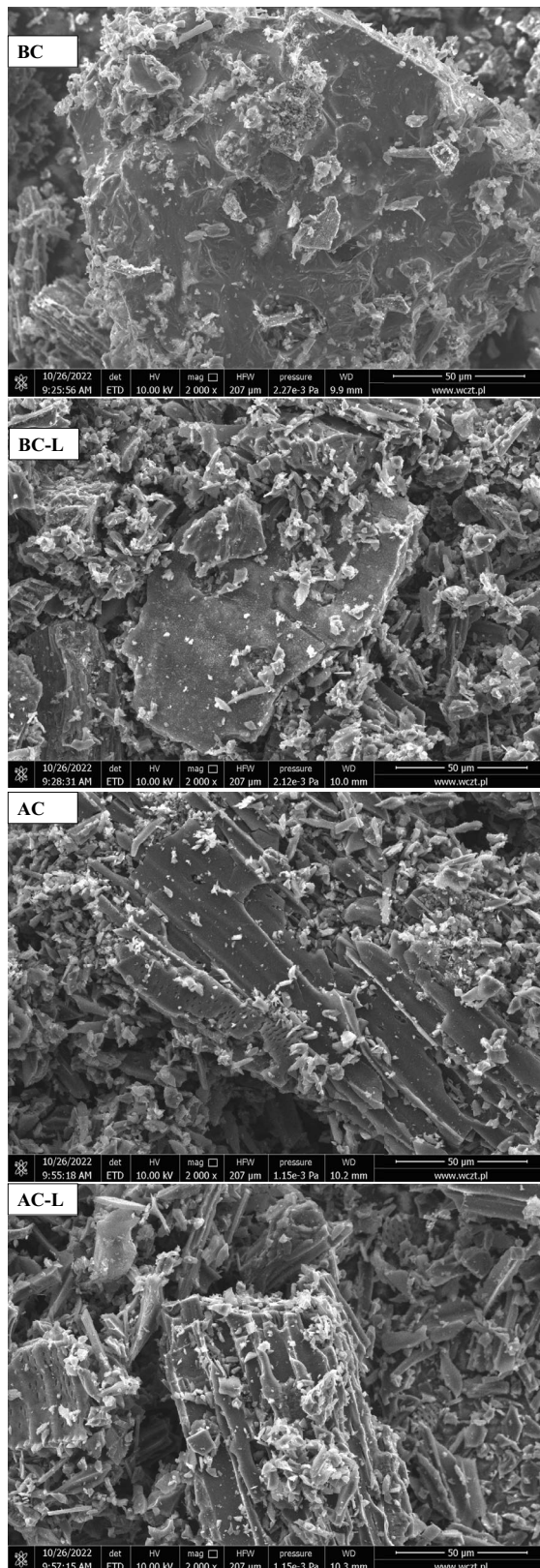
References

- [1] D. Woolf, J.E. Amonette, F.A. Street-Perrott, J. Lehmann, S. Joseph, Sustainable biochar to mitigate global climate change, *Nat. Commun.*, 1 (2010) 56, doi: 10.1038/ncomms1053.
- [2] J. Lehmann, S. Joseph, *Biochar for Environmental Management: Science, Technology and Implementation*, Routledge, Taylor & Francis Group, Abingdon and New York, 2015.
- [3] D. Xu, L. Yang, K. Ding, Y. Zhang, W. Gao, Y. Huang, H. Sun, X. Hu, S.S.A. Syed-Hassan, S. Zhang, H. Zhang, Mini-review on char catalysts for tar reforming during biomass gasification: the importance of char structure, *Energy Fuels*, 34 (2020) 1219–1229.
- [4] Q. Hu, J. Jung, D. Chen, K. Leong, S. Song, F. Li, B.C. Mohan, Z. Yao, A.K. Prabhakar, X.H. Lin, E.Y. Lim, L. Zhang, G. Souradeep, Y.S. Ok, H.W. Kua, S.F.Y. Li, H.T.W. Tan, Y. Dai, Y.W. Tong, Y. Peng, S. Joseph, C.H. Wang, Biochar industry to circular economy, *Sci. Total Environ.*, 757 (2021) 143820, doi: 10.1016/j.scitotenv.2020.143820.
- [5] E.F. Zama, B.J. Reid, H.P.H. Arp, G.X. Sun, H.Y. Yuan, Y.G. Zhu, Advances in research on the use of biochar in soil for remediation: a review, *J. Soils Sediments*, 18 (2018) 2433–2450.
- [6] J. Yuan, Y. Wen, D.D. Dionysiou, V.K. Sharma, X. Ma, Biochar as a novel carbon-negative electron source and mediator: electron exchange capacity (EEC) and environmentally persistent free radicals (EPFRs): a review, *Chem. Eng. J.*, 429 (2022) 132313, doi: 10.1016/j.cej.2021.132313.
- [7] A.M. Dehkhoda, N. Ellis, E. Gyenge, Effect of activated biochar porous structure on the capacitive deionization of NaCl and ZnCl₂ solutions, *Microporous Mesoporous Mater.*, 224 (2016) 217–228.
- [8] W.J. Liu, H. Jiang, H.Q. Yu, Emerging applications of biochar-based materials for energy storage and conversion, *Energy Environ. Sci.*, 12 (2019) 1751–1779.
- [9] J. Lim, Y.U. Shin, S. Hong, Enhanced capacitive deionization using a biochar-integrated novel flow-electrode, *Desalination*, 528 (2022) 115636, doi: 10.1016/j.desal.2022.115636.
- [10] F. Srocke, L. Han, P. Dutilleul, X. Xiao, D.L. Smith, O. Mašek, Synchrotron X-ray microtomography and multifractal analysis for the characterization of pore structure and distribution in softwood pellet biochar, *Biochar*, 1 (2021) 3, doi: 10.1007/s42773-021-00104-3.
- [11] K. Weber, P. Quicker, Properties of biochar, *Fuel*, 217 (2018) 240–261.
- [12] S. Il Jeon, H.R. Park, J.G. Yeo, S. Yang, C.H. Cho, M.H. Han, D.K. Kim, Desalination via a new membrane capacitive deionization process utilizing flow-electrodes, *Energy Environ. Sci.*, 6 (2013) 1471–1475.
- [13] C. Zhang, J. Ma, L. Wu, J. Sun, L. Wang, T. Li, T.D. Waite, Flow electrode capacitive deionization (FCDI): recent developments, environmental applications, and future perspectives, *Environ. Sci. Technol.*, 55 (2021) 4243–4267.
- [14] F. Yang, Y. He, L. Rosentsvit, M.E. Suss, X. Zhang, T. Gao, P. Liang, Flow-electrode capacitive deionization: a review and new perspectives, *Water Res.*, 200 (2021) 117222, doi: 10.1016/j.watres.2021.117222.

- [15] F. Yu, Z. Yang, Y. Cheng, S. Xing, Y. Wang, J. Ma, A comprehensive review on flow-electrode capacitive deionization: design, active material and environmental application, *Sep. Purif. Technol.*, 281 (2022) 119870, doi: 10.1016/j.seppur.2021.119870.
- [16] S. Yang, J. Choi, J.G. Yeo, S. Il Jeon, H.R. Park, D.K. Kim, Flow-electrode capacitive deionization using an aqueous electrolyte with a high salt concentration, *Environ. Sci. Technol.*, 50 (2016) 5892–5899.
- [17] A. Rommerskirchen, A. Kalde, C.J. Linnartz, L. Bongers, G. Linz, M. Wessling, Unraveling charge transport in carbon flow-electrodes: performance prediction for desalination applications, *Carbon N. Y.*, 145 (2019) 507–520.
- [18] S. Porada, D. Weingarth, H.V.M. Hamelers, M. Bryjak, V. Presser, P.M. Biesheuvel, Carbon flow electrodes for continuous operation of capacitive deionization and capacitive mixing energy generation, *J. Mater. Chem. A*, 2 (2014) 9313–9321.
- [19] K. Tang, S. Yiacoumi, Y. Li, C. Tsouris, Enhanced water desalination by increasing the electroconductivity of carbon powders for high-performance flow-electrode capacitive deionization, *ACS Sustainable Chem. Eng.*, 7 (2018) 1085–1094.
- [20] K.S. Ngai, *Electrode Materials for Electrochemical Double-Layer Capacitors*, LF. Cabeza, Ed., *Encyclopedia of Energy Storage*, Elsevier, 2022, pp. 341–350, ISBN 9780128197301. Available at: <https://doi.org/10.1016/B978-0-12-819723-3.00108-6>
- [21] G. Ravenni, O.H. Elhami, J. Ahrenfeldt, U.B. Henriksen, Y. Neubauer, Adsorption and decomposition of tar model compounds over the surface of gasification char and active carbon within the temperature range 250°C–800°C, *Appl. Energy*, 241 (2019) 139–151.
- [22] S. Dahiya, B.K. Mishra, Enhancing understandability and performance of flow electrode capacitive deionisation by optimizing configurational and operational parameters: a review on recent progress, *Sep. Purif. Technol.*, 240 (2020) 116660, doi: 10.1016/j.seppur.2020.116660.
- [23] K.B. Hatzell, M.C. Hatzell, K.M. Cook, M. Boota, G.M. Housel, A. McBride, E.C. Kumbur, Y. Gogotsi, Effect of oxidation of carbon material on suspension electrodes for flow electrode capacitive deionization, *Environ. Sci. Technol.*, 49 (2015) 3040–3047.
- [24] D.V. Cuong, P.C. Wu, N.L. Liu, C.H. Hou, Hierarchical porous carbon derived from activated biochar as an eco-friendly electrode for the electrosorption of inorganic ions, *Sep. Purif. Technol.*, 242 (2020) 116813, doi: 10.1016/j.seppur.2020.116813.
- [25] S. Porada, R. Zhao, A. Van Der Wal, V. Presser, P.M. Biesheuvel, Review on the science and technology of water desalination by capacitive deionization, *Prog. Mater. Sci.*, 58 (2013) 1388–1442.
- [26] Y. Shen, Chars as carbonaceous adsorbents/catalysts for tar elimination during biomass pyrolysis or gasification, *Renewable Sustainable Energy Rev.*, 43 (2015) 281–295.
- [27] L. Tschansky, E.R. Graber, Methodological limitations to determining acidic groups at biochar surfaces via the Boehm titration, *Carbon N. Y.*, 66 (2014) 730–733.
- [28] N.B. Klinghoffer, M.J. Castaldi, A. Nzihou, Influence of char composition and inorganics on catalytic activity of char from biomass gasification, *Fuel*, 157 (2015) 37–47.
- [29] D. Feng, H. Sun, Y. Ma, S. Sun, Y. Zhao, D. Guo, G. Chang, X. Lai, J. Wu, H. Tan, Catalytic mechanism of K and Ca on the volatile-biochar interaction for rapid pyrolysis of biomass: experimental and simulation studies, *Energy Fuels*, 34 (2020) 9741–9753.
- [30] J. Ahrenfeldt, U. Henriksen, T.K. Jensen, B. Gøbel, L. Wiese, A. Kather, H. Egsgaard, Validation of a continuous combined heat and power (CHP) operation of a two-stage biomass gasifier, *Energy Fuels*, 20 (2006) 2672–2680.
- [31] J. Jagiełło, Stable numerical solution of the adsorption integral equation using splines, *Langmuir*, 10 (2002) 2778–2785.
- [32] J. Jagiełło, J.P. Olivier, 2D-NLDFT adsorption models for carbon slit-shaped pores with surface energetical heterogeneity and geometrical corrugation, *Carbon N. Y.*, 55 (2013) 70–80.
- [33] J. Bitenc, A. Vizintin, J. Grdadolnik, R. Dominko, Tracking electrochemical reactions inside organic electrodes by operando IR spectroscopy, *Energy Storage Mater.*, 21 (2019) 347–353.
- [34] M. Ilić, F.H. Haegel, A. Lolić, Z. Nedić, T. Tosti, I.S. Ignjatović, A. Linden, N.D. Jablonowski, H. Hartmann, Surface functional groups and degree of carbonization of selected chars from different processes and feedstock, *PLoS One*, 17 (2022) e0277365, doi: 10.1371/JOURNAL.PONE.0277365.
- [35] C. Qin, H. Wang, X. Yuan, T. Xiong, J. Zhang, J. Zhang, Understanding structure-performance correlation of biochar materials in environmental remediation and electrochemical devices, *Chem. Eng. J.*, 382 (2020) 122977, doi: 10.1016/j.cej.2019.122977.
- [36] A. Dufour, A. Celzard, V. Fierro, E. Martin, F. Broust, A. Zoulalian, Catalytic decomposition of methane over a wood char concurrently activated by a pyrolysis gas, *Appl. Catal., A*, 346 (2008) 164–173.
- [37] D. Boonpakdee, C.F. Guajardo Yévenes, W. Surareungchai, C. La-O-Vorakiat, Exploring non-linearities of carbon-based microsupercapacitors from an equivalent circuit perspective, *J. Mater. Chem. A*, 6 (2018) 7162–7167.
- [38] M. Forghani, S.W. Donne, Method comparison for deconvoluting capacitive and pseudo-capacitive contributions to electrochemical capacitor electrode behavior, *J. Electrochem. Soc.*, 165 (2018) A664–A673.
- [39] S. Bhattacharjee, DLS and zeta potential – What they are and what they are not?, *J. Control Release*, 235 (2016) 337–351.
- [40] D. Biriukov, P. Fibich, M. Předota, Zeta potential determination from molecular simulations, *J. Phys. Chem. C*, 124 (2020) 3159–3170.
- [41] T.F. Tadros, Ed., Volume 1 Basic Principles of Interface Science and Colloid Stability, De Gruyter, n.d. <https://doi.org/doi:10.1515/9783110540895>.
- [42] J. Ma, C. He, D. He, C. Zhang, T.D. Waite, Analysis of capacitive and electrochemical contributions to water desalination by flow-electrode CDI, *Water Res.*, 144 (2018) 296–303.
- [43] K. Alsaikhan, A. Al Sultan, A. Alkhalidi, A. Bentalib, A. Abutalib, D. Wu, J. Li, R. Xie, Z. Peng, M. Khamis, I. Wait, V. Nenov, Carbon material-based flow-electrode capacitive deionization for continuous water desalination, *Processes*, 11 (2023) 195, doi: 10.3390/PR11010195.
- [44] J.H. Choi, Determination of the electrode potential causing Faradaic reactions in membrane capacitive deionization, *Desalination*, 347 (2014) 224–229.
- [45] P. Nativ, Y. Badash, Y. Gendel, New insights into the mechanism of flow-electrode capacitive deionization, *Electrochem. Commun.*, 76 (2017) 24–28.
- [46] C. Zhang, D. He, J. Ma, W. Tang, T.D. Waite, Faradaic reactions in capacitive deionization (CDI) - problems and possibilities: a review, *Water Res.*, 128 (2018) 314–330.
- [47] I. Cohen, E. Avraham, Y. Bouhadana, A. Soffer, D. Aurbach, Long term stability of capacitive de-ionization processes for water desalination: the challenge of positive electrodes corrosion, *Electrochim. Acta*, 106 (2013) 91–100.
- [48] J.R. Rumble, D.R. Lide, T.J. Bruno, *CRC Handbook of Chemistry and Physics [2019–2020]: A Ready-Reference Book of Chemical and Physical Data*, CRC Press, Boca Raton, 2019.
- [49] A. Rommerskirchen, C.J. Linnartz, F. Egidi, S. Kendir, M. Wessling, Flow-electrode capacitive deionization enables continuous and energy-efficient brine concentration, *Desalination*, 490 (2020) 114453, doi: 10.1016/j.desal.2020.114453.
- [50] X. Ruan, Y. Sun, W. Du, Y. Tang, Q. Liu, Z. Zhang, W. Doherty, R.L. Frost, G. Qian, D.C.W. Tsang, Formation, characteristics, and applications of environmentally persistent free radicals in biochars: a review, *Bioresour. Technol.*, 281 (2019) 457–468.
- [51] Y. Liu, M. Paskevicius, M.V. Sofianos, G. Parkinson, S. Wang, C.Z. Li, A SAXS study of the pore structure evolution in biochar during gasification in H₂O, CO₂ and H₂O/CO₂, *Fuel*, 292 (2021) 120384, doi: 10.1016/j.fuel.2021.120384.

Supporting information

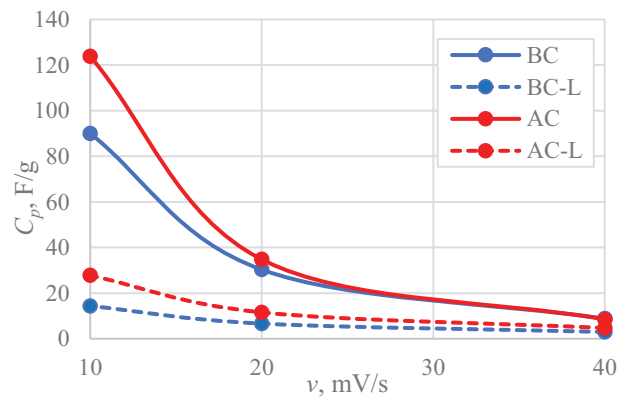
S1. SEM micrographs of raw (BC, AC) and leached (BC-L, AC-L) carbons



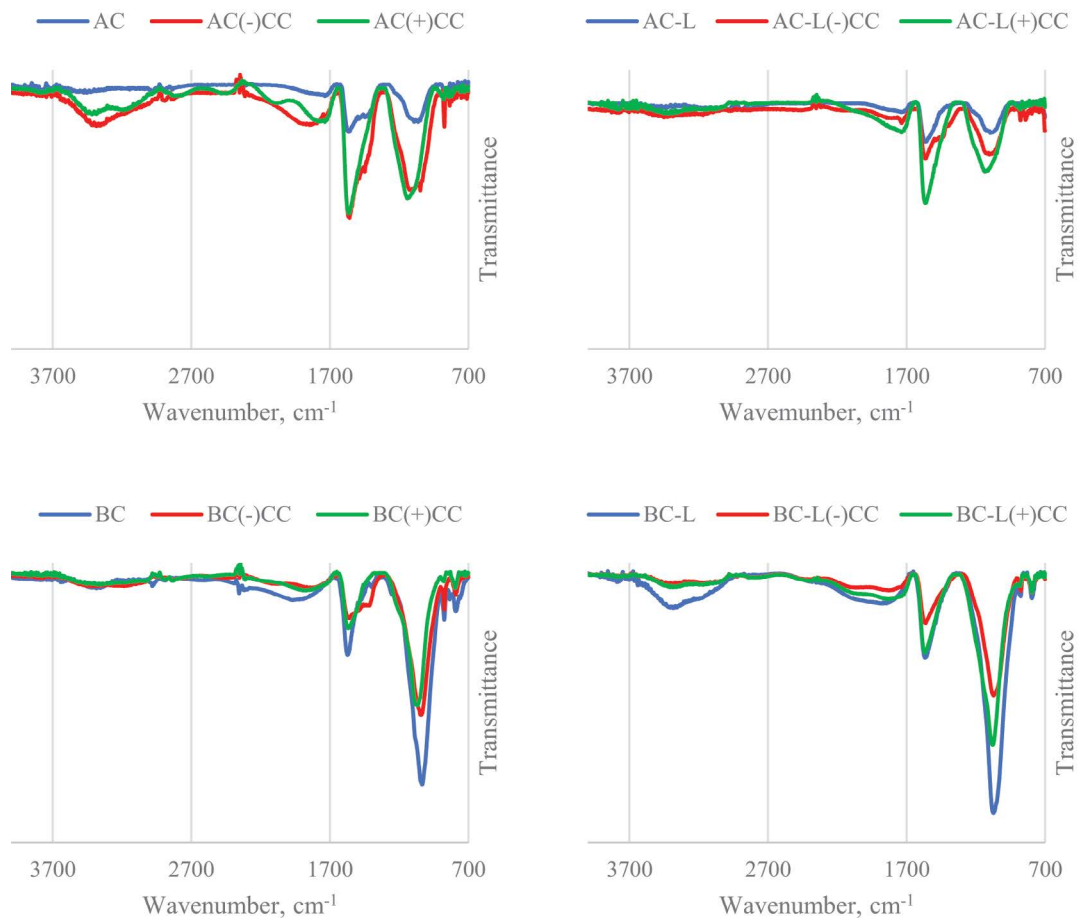
S2. Atomic composition (At.%) of the carbon surface based on SEM-EDS analysis

	C	O	Na	Mg	Al	Si	P	S	Cl	K	Ca	Fe
BC	43.90	32.08	0.34	0.51	0.12	11.05	0.36	0.03	0.09	3.11	1.63	6.68
BC-L	77.15	17.87	nd	0.33	0.01	4.16	0.06	0.10	0.01	0.05	0.21	nd
AC	95.67	3.98	nd	0.01	nd	nd	0.02	0.01	nd	0.03	0.28	nd
AC-L	96.35	3.54	0.01	nd	nd	nd	nd	nd	0.05	nd	0.05	nd

S3. Specific capacitance change with scan rate



S4. FTIR spectra of the carbons after working as cathode (-) and anode (+) during the C.C. mode



S5. Final pH of process solutions in FCDI experiments

Operational mode	Carbon material	Cathode	Anode	Diluate
C.V.	None (ED)	7.94	3.19	6.71
	AC	10.79	8.12	6.07
	AC-L	11.98	2.03	7.36
	BC	11.25	9.4	7.81
	BC-L	10.65	6.8	7.51
C.C.	None (ED)	12.51	1.73	3.42
	AC	12.35	1.89	3.84
	AC-L	12.29	1.56	3.41
	BC	12.36	6.48	4.04
	BC-L	12.23	1.72	3.57

S6. pH of carbon materials in study after 24 h of shaking in deionized water or 3%wt NaCl solution

